Water Supply

IWA PUBLISHING

Water Supply Vol 22 No 4, 4400 doi: 10.2166/ws.2022.058

Discharge modeling in compound channels with non-prismatic floodplains using GMDH and MARS models

Hojjat Allah Yonesi [a,*], Abbas Parsaie[b], Azadeh Arshia[a] and Zahra Shamsi[a]

[a] Water Engineering Department, Lorestan University, Khorramabad, Iran
[b] Faculty of Water Sciences Engineering, Shahid Chamran University of Ahvaz, Ahvaz, Iran
*Corresponding author. E-mail: yonesi.h@lu.ac.ir

HAY, 0000-0002-5145-6185

ABSTRACT

In this study, modeling of discharge was performed in compound open channels with non-prismatic floodplains (CCNPF) using soft computation models including multivariate adaptive regression splines (MARS) and group method of data handling (GMDH), and then their results were compared with the multilayer perceptron neural networks (MLPNN). In addition to the total discharge, the discharge separation between the floodplain and main channel was modeled and predicted. The parameters of relative roughness coefficient, the relative area of flow cross-section, relative hydraulic radius, bed slope, the relative width of water surface, relative depth, convergence or divergence angle, relative longitudinal distance as inputs, and discharge were considered as models output. The results demonstrated that the statistical indices of MARS, GMDH, and MLPNN models in the testing stage are $R^2 = 0.962$(RMSE = 0.003), 0.930(RMSE = 0.004), and 0.933(RMSE = 0.004) respectively. Examination of statistical error indices shows that all the developed models have the appropriate accuracy to estimate the flow discharge in CCNPF. Examination of the structure of developed GMDH and MARS models demonstrated that the relative parameters: roughness, area, hydraulic radius, flow aspect ratio, depth, and angle of convergence or divergence of floodplain have the greatest impact on modeling and estimation of discharge.

Key words: discharge estimation, non-prismatic compound open channels, soft computing models

HIGHLIGHTS

- Estimation of discharge was performed in compound open channels with non-prismatic floodplains using soft computation models.
- Discharge separation between the floodplain and main channel was predicted.
- Effective parameters for determining the discharge are introduced.
- The accuracy of each of the methods is calculated.
- The performance of the developed models was compared with the ANFIS model.

NOTATIONS

ANFIS	adaptive neuro-fuzzy inference system
A_r	relative area
CCNPF	compound open channel with non-prismatic floodplains
f_r	relative roughness
GMDH	group method of data handling
MARS	multivariate adaptive regression splines
MLPNN	multilayer perceptron neural networks
R^2	coefficient of determination
RMSE	root mean square error
R_r	relative hydraulic radius
S_0	bed slope
SVM	support vector machine
x_r	relative longitudinal distance

θ	convergence or divergence angle
α	relative width
Dr	relative flow depth
δ^*	flow aspect ratio

INTRODUCTION

Rivers are one of the most important resources of water for agriculture, industry, and drinking. Easy access and availability have led to the formation of human civilizations in their neighborhood for a long time (Torfi *et al.* 2021). Also, some industrial projects have been built near rivers to reduce water transfer costs. Floods are one of the most dangerous natural disasters that occur in river sections. These phenomena with different recurrence periods (from low-flow floods to high-flow floods), can cause very serious damage to human communities, agricultural lands, and industrial projects. The study of river hydraulics is the first important step in the study and control of floods (Graf & Altinakar 1998; Dingman 2009). In estimating damages due to floods, estimating the discharge in the floodplains and the main section is very important. By the estimation of flow discharge in floodplains, the depth, flooding zone, and also the time of submergence of the floodplains can be estimated.

Normally, the stream flows in its main channel in the river, but in flood conditions, the stream leaves its bed and enters the surrounding areas (floodplains). In this condition, the cross-section of the stream consists of the main channel and floodplains. As the flow enters the floodplains, its properties differ from the single channel. For example, the velocity in floodplains is lower than the main channel, and their roughness is higher than the main channel (Bousmar *et al.* 2006). The difference in velocity in these regions leads to shear stresses and vortices at the boundary between the main channel and the floodplains. In the past two decades, good efforts have been made to more accurately simulate hydraulics of flood in compound sections at rivers. In compound open channel hydraulics, the flow characteristics at the main channel and floodplains as well as their interaction with each other are considered. So far, many types of research have been conducted on the hydraulics of flow in compound open channels (Roushangar *et al.* 2021). Most of them have focused on determining the relation between stage-discharge, velocity distribution (Knight & Demetriou 1983), and shear stress in the main channel and floodplains, secondary flow, and turbulence characteristics. Sellin (1964) showed that the interaction of the flow in the main channel and the floodplains cause vortices in their common boundary, which cause the head loss of flow, and consequently the total flow rate is reduced. Mohanty *et al.* (2011) investigated the shear stress changes in the compound open channel focusing on the boundary range between the main channel and the floodplain. Their studies demonstrated that the shear layer depends on the geometric and hydraulic conditions of the flow. By increasing the ratio of floodplain width to the width of the main channel, the shear layer expansion range decreases, and with the decrease of the ratio of the flow depth in the main channel to the floodplain, it will increase. Parsaie *et al.* (2016) investigated the accuracy of empirical models including the unit cross-section method, divided channel method (DCM), and coherence method using laboratory and field data. They stated that the divided channel method works well by considering the virtual vertical line as the dividing line between the sub-sections (main channel and floodplains) and can be used for practical problems. Changes in the geometry of the flow section along the river's path cause the cross-section to be non-prismatic and change the flow from uniform to non-uniform.

In other words, the hydraulic complexity of the compound open channel flow increases when the width of the cross-section changes and the compound channel section changes from prismatic to non-prismatic. Bousmar *et al.* (2006) investigated the hydraulic flow in a compound channel with convergent floodplains. Their findings demonstrated that at high relative depths, the lateral mass transfer in the final half of the convergent region is higher than the initial half region.

Rezaei & Knight (2009) investigated the accuracy of the Shiono & Knight's model (SKM) (1988, 1991) in compound channels with non-prismatic sections. They stated that the SKM model does not have an appropriate accuracy for hydraulic modeling of flow in such sections. For this purpose, they modified the SKM model and the modified Shiono Knight model (M-SKM) to estimate the flow parameters including average depth velocity, boundary shear stress, and determining the stage-discharge relation. Naik *et al.* (2014) conducted a laboratory study of hydraulic flow in a compound channel with non-prismatic floodplains. The results of their research demonstrated that the depth average velocity and boundary shear stress increase during the convergence region. Today, flow characteristics in prismatic compound open channels are estimated using soft computing models and mathematical modeling.

For example, discharge in prismatic compound channels using artificial neural network models, support vector machine models, fuzzy adaptive neural network (Najafzadeh & Zahiri 2015; Parsaie *et al.* 2017), and multivariate adaptive spline

regression method (Parsaie & Haghiabi 2017) and gene expression programming (Azamathulla & Zahiri 2012) have been modeled with great accuracy. Also prediction of depth-averaged velocity distribution of compound channels with converging flood plains using Fluent software and artificial neural network has been performed (Naik *et al.* 2017). In another study, Singh *et al.*(2019) used gene expression and a back propagation neural network to investigate the apparent shear stress in an asymmetric compound channel. The results of their research showed that the formulas produced by these two models provide very satisfactory results compared to previous models. Singh & Tang (2020), using the neuro-fuzzy inference system, predicted the apparent shear stress values in an asymmetric compound channel with five geometrical and hydraulic parameters with appropriate accuracy. The discharge in meandering compound channels has also been estimated by Mohanta *et al.* (2020) and Pradhan & Khatua (2019a) using empirical models. Using soft computing models the research to date has tended to focus on estimating discharge in compound channels with prismatic floodplains rather than non-prismatic floodplains. In other words, little research has been done on non-uniform sections (Pradhan & Khatua 2019b; Mohanta & Patra 2021) or compound open channels with non-prismatic floodplains (CCNPF; Das *et al.* 2020). Hence, due to the importance of discharge estimation especially in flood conditions, in this study, in addition to estimating the total flow rate, discharge prediction is considered in the floodplain and the main channel.

The present study fills a gap in the literature by using soft computation models. These models include the group method of data handling and multivariate adaptive spline regression method, modeling and estimating discharge in compound CCNPF. Also with using these models, the percentage of participation of discharge in the floodplains and the main channel has been estimated.

METHODOLOGIES

This section introduces the important parameters involved in predicting the discharge in non-prismatic compound open channels and then defines the statistical properties of the collected data and related sources. Finally, the soft computing models used in this research, which include multivariate adaptive regression splines (MARS), GMDH, and multilayer perceptron neural networks (MLPNN) will be introduced.

NON-PRISMATIC COMPOUND OPEN CHANNELS

A view of non-prismatic compound open channels including convergent or divergent floodplains is shown in Figure 1. By examining the hydraulics of the flow in non-prismatic compound open channels, the researchers found that the flow in the compound channel depends on the coefficient of friction, area ratio, width ratio, ratio of the hydraulic radius, relative

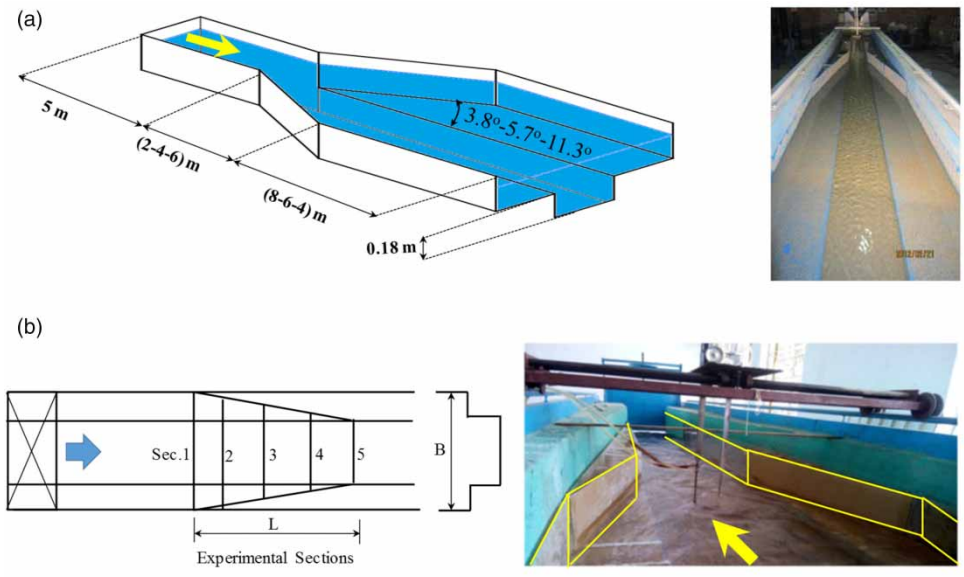

Figure 1 | View of a non-prismatic compound channel (a) divergent floodplain (b) convergent floodplain.

longitudinal distance, relative depth, flow aspect ratio, and bed slope. Hence, in this present study, for developing the MLPNN, GMDH, and MARS models, nine dimensionless input parameters presented in Equation (1) were considered.

$$Q = \psi(f_r,\ A_r,\ R_r,\ Dr,\ S_0,\ \delta^*,\ \alpha,\ \theta,\ x_r) \tag{1}$$

where, $f_r = f_{mc}/f_{fp}$ = relative roughness with f_{mc}, f_{fp} = the main channel and floodplain Darcy-Wiesbach friction factor,respectively; $A_r = A_{mc}/A_{fp}$ = relative area with A_{mc}, A_{fp} = the main channel and floodplain cross section, respectively; $R_r = R_{mc}/R_{fp}$ = relative hydraulic radius with R_{mc}, R_{fp} = hydraulic radius of the main channel and floodplain, respectively; $\delta^* = b/H$ = flow aspect ratio(main channel width to the total flow depth); $\alpha = B/b$ = relative width(width of the floodplain to the width of the main channel); $Dr = (H - h)/H$ = relative flow depth(h is bankfull depth); $x_r = l/L$ = relative longitudinal distance with l, L = distance of any point from beginning of the divergent or convergent and total length of divergent or convergent region, respectively; θ = convergence or divergence angle and S_0 = bed slope.

To develop the mentioned artificial intelligence models, laboratory data of Othman (2000), Bousmar (2002), Rezaei & Knight (2009), Yonesi *et al.* (2013), and Naik & Khatua (2016) have been used. Table 1 shows the statistical characteristics of the collected data.

Review of MLPNN

A neural network is an advanced non-linear mathematical model that can simulate the relationship between the inputs and outputs of a complex non-linear system. In many simulations that lead to the solution of complex equations to find the relation between the factors affecting the system, a neural network can be used as a suitable alternative. The MLPNN is one of the most widely used types of ANN models. Figure 2 shows a view of this model. As shown in this figure, the inputs of the neural network model are multiplied by coefficients (w: weight) and then those are added by a constant value (b: bias). The transfer function is then added to the result. The design of an MLPNN model consists of several steps, which are: defining the number of model layers including the input layer, hidden layer(s), an output layer, number of neurons in each layer, defining the active transfer function, and finally choosing the training method. Neural network training means determining the values of weights and constants that are multiplied and added to each input. Various methods for neural network training have been proposed, such as reduction gradient methods, Levenberg–Marquardt algorithm, or metaheuristic methods such as genetic algorithm and particle swarm optimization. In the metaheuristic methods, neural network training is assumed as an optimization problem (Sihag *et al.* 2021).

Table 1 | Statistical characteristics of the collected data

	f_r	A_r	R_r	Dr	S_0	δ*	α	x_r	θ	Q
Minimum	0.31	0.93	1.70	0.11	0.0009	1.41	1.33	0.00	−13.38	0.01
Maximum	0.84	22.59	35.09	0.54	0.0020	6.54	3.02	1.00	11.31	0.06
Range	0.53	21.66	33.39	0.43	0.0011	5.13	1.69	1.00	24.69	0.05
Mean	0.70	4.37	3.51	0.34	0.0012	4.40	2.10	0.42	−2.17	0.02
Median	0.71	3.01	2.80	0.33	0.0010	4.19	2.00	0.33	−1.91	0.02
First quartile	0.65	1.86	2.30	0.25	0.0010	3.77	1.67	0.17	−9.00	0.02
Third quartile	0.76	5.58	3.73	0.44	0.0011	5.38	2.51	0.67	3.81	0.04
Variance	0.01	13.86	9.89	0.01	0.0000	1.62	0.30	0.10	48.85	0.00
Average deviation	0.07	2.70	1.43	0.10	0.0003	1.04	0.47	0.28	6.01	0.01
Standard deviation	0.09	3.72	3.14	0.12	0.0004	1.27	0.55	0.32	6.99	0.01
Coefficient of variation	0.13	0.85	0.90	0.35	0.3440	0.29	0.26	0.77	−3.22	0.56
Skew	−1.06	2.09	6.57	0.19	1.2530	−0.61	0.32	0.32	−0.06	1.15
Kurtosis	2.03	5.58	55.13	−0.99	−0.3250	−0.02	−1.11	−1.13	−1.17	0.52

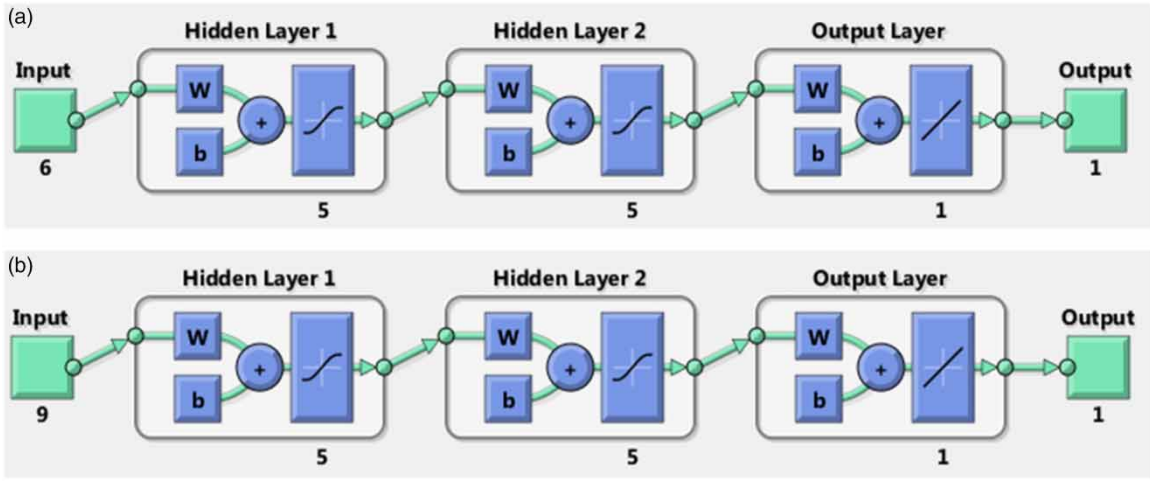

Figure 2 | The structure of the MLPNN developed to estimate the discharge in the compound open channel with non-prismatic floodplains (a) 6 inuts (b) 9 inputs.

Review of GMDH

The GMDH model is one of the a posteriori approaches based on perceptron theory. This approach has been developed to identify, model, and predict complex systems (Najafzadeh & Azamathulla 2015). GMDH is a combination of adlines, and modified versions of this method have been used for various modeling applications. This method has higher accuracy compared with the perceptron-type structure because in this model, the division of information into two categories of useful and non-useful is used. GMDH also requires less observational data (Ivakhnenko 1971). Figure 3 shows the structure of the GMDH network developed with a quadratic polynomial as the activation function (Equation (2)) in this study to model and prediction of flow discharge in the non-prismatic compound open channels (Bhoria *et al.* 2021).

The network structure is determined by the proposed algorithm as follows: selection of input variables to the model, collecting of a set of observational data related to the subject, dividing of the data into two groups: calibration and validation data, building N-adline for all two pairs of input variables, the transfer function for each neuron, estimate the weighting coefficients for all N-adlines by least squares error method (LSE), calculation of filtration criteria, comparison of calculated criteria for all N-adlines with a set threshold value. If the threshold value is greater than the filtration criteria, the M-adline is removed. Then other adlines remain for the next layer. A fixed threshold value can be considered for all layers or a threshold value for each layer.

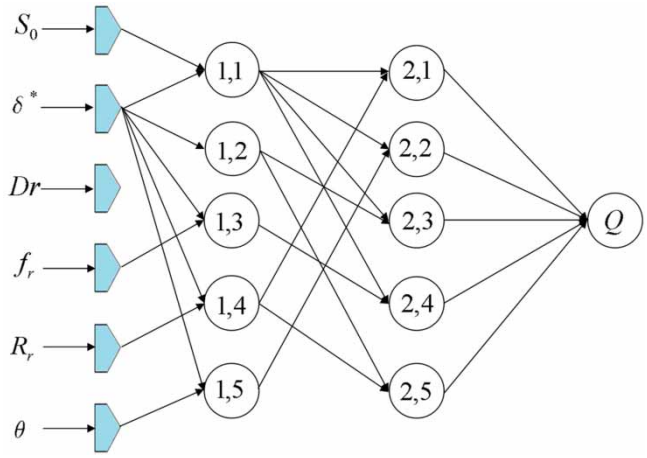

Figure 3 | The structure of the developed GMDH model with 6 inputs to estimate the discharge in a non-prismatic compound channel.

Each neuron in the GMDH structure performs a non-linear function of the inputs. This non-linear function is as follows:

$$Y = w_0 + w_1x_1 + w_2x_2 + w_3x_1^2 + w_4x_2^2 + w_5x_1x_2 \tag{2}$$

where w_0 to w_5 is the weight of the parameters and x_1, x_2 are the input variables. Using the LSE method, six coefficients are calculated for each neuron. The steps of which are as follows: a set of 6 coefficients must be found for each neuron so that the mean squared error between the neurons' outputs is y_n and the actual value of φ_n is minimum.

$$\begin{aligned}
\phi_1 &= w_0 + w_1x_{1i} + w_2x_{1j} + w_3x_{1i}^2 + w_4x_{1j}^2 + w_5x_{1i}x_{1j} \\
\phi_2 &= w_0 + w_1x_{2i} + w_2x_{2j} + w_3x_{2i}^2 + w_4x_{2j}^2 + w_5x_{2i}x_{2j} \\
&\vdots \\
\phi_N &= w_0 + w_1x_{Ni} + w_2x_{Nj} + w_3x_{Ni}^2 + w_4x_{Nj}^2 + w_5x_{Ni}x_{Nj}
\end{aligned} \tag{3}$$

That this equation is written as the following general matrix:

$$\phi = XW \tag{4}$$

Matrixes ϕ, X and W have dimensions N × 1, N × 6, and 6 × 1, respectively. Normal equations are obtained by multiplying both sides of Equation (4) in the matrix X transposition:

$$X^T\phi = (X^TX)\,W \quad \Rightarrow W = (X^TX)^{-1}X^T\phi \tag{5}$$

X^TX is a 6 × 6 matrix and the coefficients can be obtained using the inverse method. The W matrix consists of a set of 6 coefficients. This matrix can approximate correct outputs with a minimum mean square error. The above steps are repeated for all the first layer neurons as well as for all subsequent layer neurons. The neuron's performance function is determined after obtaining six coefficients. This performance function is controlled by correlating or calculating the mean square error between the actual data outputs. Finally, to continue the solution, neurons with a performance function higher than the threshold value are selected (Najafzadeh *et al.* 2013; Najafzadeh & Azamathulla 2015; Najafzadeh & Sattar 2015).

Review of MARS method

The MARS method first was proposed by Friedman (1991) to predict continuous numerical outputs. This model is one of the local non-parametric models. The application of the non-parametric term in this model is that the structure of the model is not known before modeling. Also, the MARS model not only does not use all data together but also divides data into subcategories and then performs the modeling operation for each of these subcategories. The mathematical models of such subcategories are local. In the MARS model, it is possible to find a hidden non-linear pattern in a data set including a large number of variables. In this method, it is possible to define the estimation function and there is no need to combine several statistical methods. This model is based on basis functions, which are defined as follows for each variable.

$$\max\{0,\ x - t\} \quad \text{and} \quad \max\{0,\ t - x\} \tag{6}$$

where t = a node and in practice is an explanatory variable. These functions are called spline functions, which are reflected in the node t-pair. The general form of the MARS model is as follows :

$$\hat{Y} = C_0 + \sum_{k=1}^{M} \beta_k\, B_k\,(X) \tag{7}$$

where $\hat{Y}$ = estimate the value of the response variable, X = vector of the explanatory variables, B_k = the basis function, and β_k = coefficients that are determined by minimizing the sum of the squares of the residuals.

Each basis function may be a spline linear function or the multiplication of two or more of them that express interactions. MARS divides the space of explanatory variables into specific regions with specific nodes. The MARS model fitting is performed in two stages, forward and backward, respectively. In the forward stage, a large number of basis functions with different nodes are continuously added to the model. In the backward stage, the basis functions that are less important and effective in estimating are removed.

Finally, the best model is selected based on a minimum criterion called 'generalized cross-validation (GCV)'. GCV_k is the k^{th} model in deleting phase. This quantity is defined by the following expression:

$$GCV_k = \frac{1}{n}\sum_{i=1}^{n}\left(y_i - \hat{f}_k(x_i)\right)^2 / (1 - C(k)/n)^2 \quad (8)$$

where $\hat{f}_k$ = estimated model in k^{th} step of backward elimination stage, and $C(k) = \lambda$. M = the number of sentences in k^{th} model, M = the number of spline function nodes in the model($2 < M < 4$), and λ = cost function criterion.

Modeling strategies

As shown in Equation (1), nine parameters can be used as input variables to model and prediction of flow discharge in a compound channel with non-prismatic floodplains using soft computing models (Figure 4). Therefore, in designing the pattern of input variables, a combination of one to nine parameters can be considered. In other words, it is possible to define the input variable by combining k ($1 < k < 9$) and $n = 9$ ($C(n, k) = n!/(n-k)k!$). Different approaches can be used in soft computing models to reduce modeling time and identify the best input combination. The first step is to use the variables that have the highest correlation with the output variable (discharge). For this purpose, the correlation of independent variables and discharge are calculated and are presented in Table 2 and Figure 5.

As can be seen from this figure and table, in the data range used, there is the highest positive correlation between Q and A_r and R_r. Also, there is a slight positive correlation with the divergence (convergence) angle. As shown in this table, the discharge is inversely related to other parameters such as the f_r and β. For finding the most effective parameters, other methods, such as the gamma test can be used (Das *et al.* 2020). This method also works based on the correlation coefficient. Such methods are used to design the input variables of the soft computing model, such as MLPNN, adaptive neuro-fuzzy inference system (ANFIS), and SVM. However, in the GMDH and MARS models, the most important influential parameters in determining the output parameter (discharge) are automatically identified in the model development process, and in the final model, the highest weight coefficient is assigned to them. In this study, for the development of the mentioned soft computing models including GMDH, MARS, MLPNN models, the collected dataset (196 datasets) was divided into two categories of training and testing.

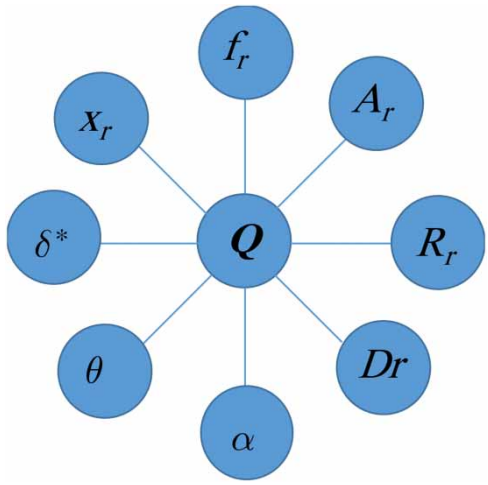

Figure 4 | Input variables for discharge estimation in CCNPF.

Table 2 | Correlation of variables involved in estimating discharge

	f_r	A_r	R_r	Dr	S_o	δ*	α	x_r	θ	Q
f_r	1.00									
A_r	−0.71	1.00								
R_r	−0.79	0.57	1.00							
Dr	0.84	−0.58	−0.49	1.00						
S_o	0.16	−0.21	−0.16	0.03	1.00					
δ*	0.12	−0.03	−0.30	−0.16	0.35	1.00				
α	0.41	−0.70	−0.26	0.20	0.27	0.05	1.00			
x_r	0.15	−0.14	−0.13	0.11	0.10	0.12	0.10	1.00		
θ	−0.09	−0.10	0.16	0.06	−0.25	−0.16	0.05	0.36	1.00	
Q	−0.34	0.22	0.31	−0.21	−0.13	−0.81	−0.14	−0.14	0.10	1.00

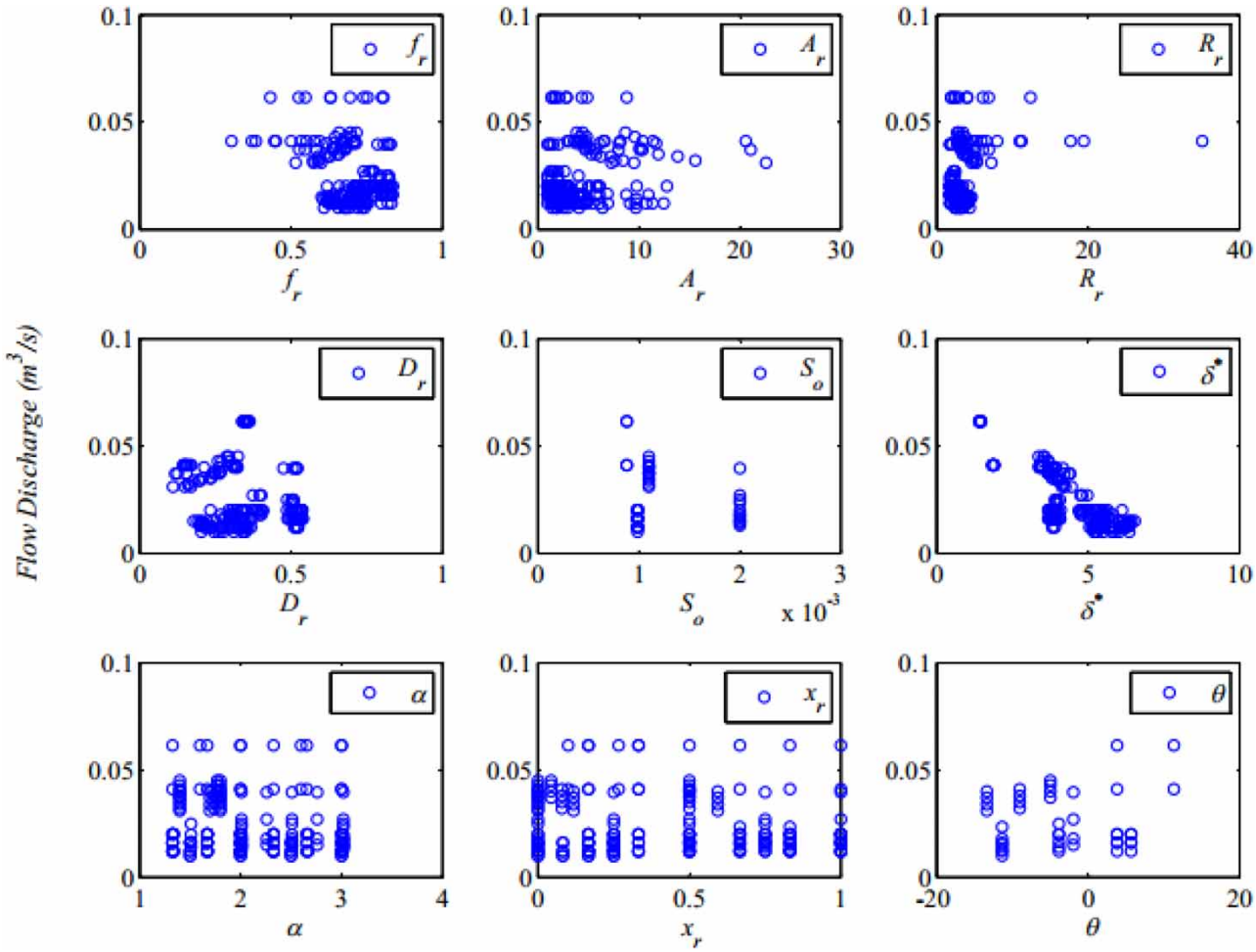

Figure 5 | Involved parameters versus discharge in CCNPF.

RESULTS AND DISCUSSION

The histogram of the data used is shown in Figure 6. Eighty percent of the data were randomly selected to model training, and the remaining 20% was devoted to testing of the model.

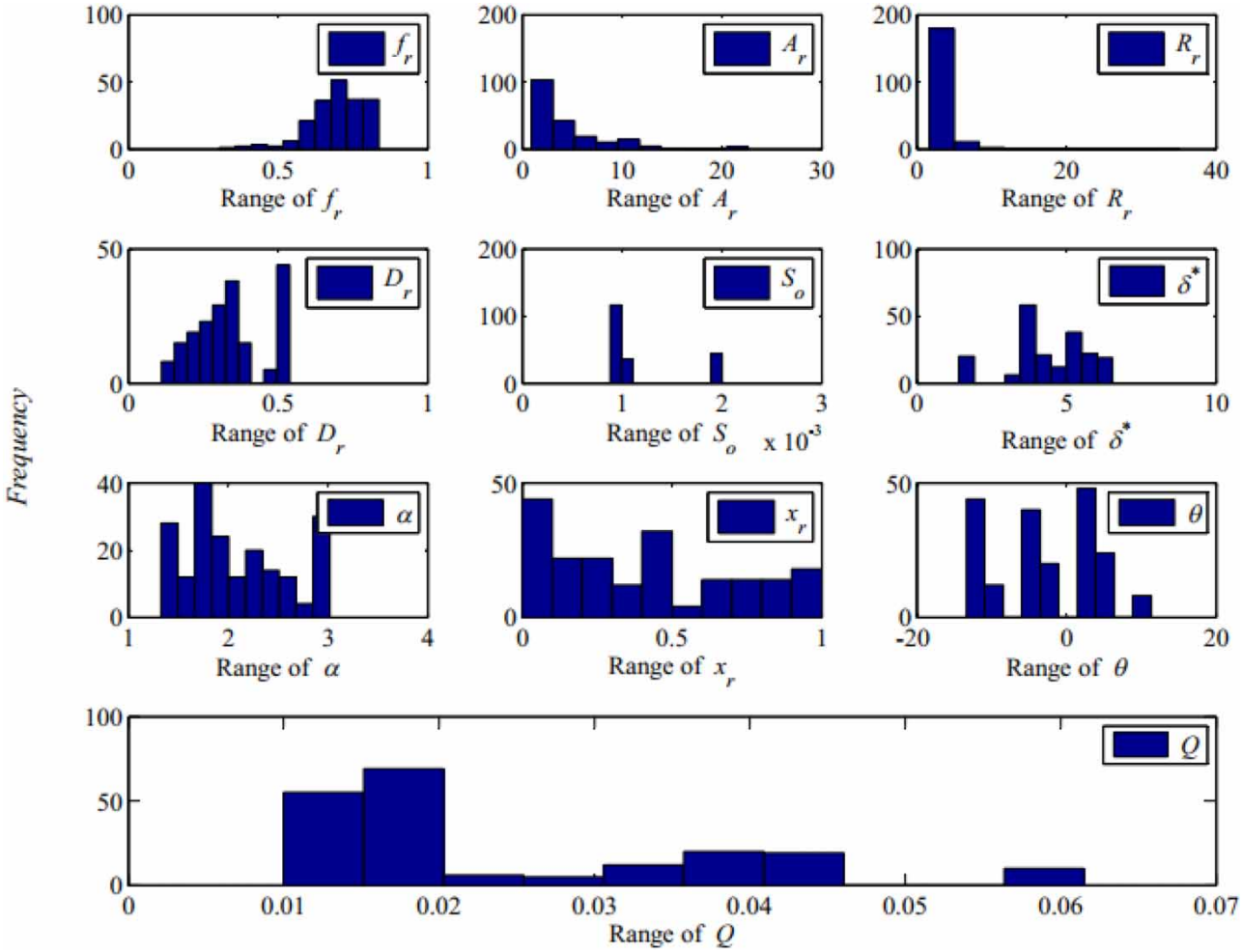

Figure 6 | Histogram of data used to estimate discharge in compound channels with non-prismatic floodplains.

The statistical characteristics of the data assigned to each of the training and testing categories are presented in Tables 3 and 4, respectively. The most important point in assigning data to each of the training and testing groups is that the range of data assigned to both categories is close to each other.

The error indices including coefficient of determination (R^2) and root mean square error (RMSE) was used to evaluate the developed models. In addition, the developed discrepancy ratio (DDR) is used for evaluating the characteristics of the developed models. Taylor diagram was used to compare the performance of the developed models. The DDR index shows the ratio of the predicted values to the observed values minus one. If the value of this index is positive, it indicates the property of overprediction, and if it is negative, it has the property of underprediction. Based on this index, in addition to its numerical values for training and test data, it is necessary to draw a histogram and its range.

$$R^2 = \left(\frac{\sum_{i=1}^{n} (O_i - \overline{O})(P_i - \overline{P})}{\sqrt{\sum_{i=1}^{n} (O_i - \overline{O})^2} \sqrt{\sum_{i=1}^{n} (P_i - \overline{P})^2}} \right)^2 \tag{9}$$

$$RMSE = \sqrt{\frac{\sum_{i=1}^{n} (O_i - P_i)^2}{n}} \tag{10}$$

Table 3 | Statistical characteristics of the data assigned to the training

	f_r	A_r	R_r	Dr	S_0	δ*	α	x_r	θ	Q
Minimum	0.38	0.93	1.70	0.11	0.00	1.41	1.33	0.00	−13.38	0.01
Maximum	0.84	22.59	17.69	0.54	0.00	6.54	3.02	1.00	11.31	0.06
Range	0.45	21.66	15.99	0.43	0.00	5.13	1.69	1.00	24.69	0.05
Mean	0.70	4.45	3.30	0.34	0.00	4.35	2.08	0.44	−2.32	0.02
Median	0.71	3.06	2.79	0.33	0.00	4.10	2.00	0.50	−1.91	0.02
First quartile	0.65	1.86	2.31	0.26	0.00	3.77	1.67	0.17	−9.00	0.02
Third quartile	0.76	5.79	3.70	0.49	0.00	5.36	2.51	0.67	3.81	0.04
Variance	0.01	13.94	3.74	0.01	0.00	1.57	0.29	0.10	48.68	0.00
Average deviation	0.07	2.75	1.15	0.10	0.00	1.01	0.46	0.28	6.07	0.01
Standard deviation	0.09	3.75	1.94	0.12	0.00	1.26	0.54	0.32	7.00	0.01
Coefficient of variation	0.01	13.94	3.74	0.01	0.00	1.57	0.29	0.10	48.68	0.00
Skew	−0.73	1.99	4.03	0.19	1.50	−0.61	0.36	0.24	−0.09	1.10
Kurtosis	0.77	5.19	23.03	−0.97	0.40	0.07	−1.05	−1.17	−1.24	0.41

Table 4 | Statistical characteristics of the data assigned to the testing

	f_r	A_r	R_r	Dr	S_0	δ*	α	x_r	θ	Q
Minimum	0.31	0.94	1.72	0.15	0.00	1.44	1.33	0.00	−13.38	0.01
Maximum	0.84	20.60	35.09	0.53	0.00	6.43	3.02	1.00	11.31	0.06
Range	0.53	19.66	33.37	0.39	0.00	4.99	1.69	1.00	24.69	0.05
Mean	0.69	4.05	4.36	0.33	0.00	4.62	2.20	0.34	−1.55	0.02
Median	0.71	2.85	2.85	0.34	0.00	4.85	2.01	0.25	−1.91	0.02
First quartile	0.64	1.92	2.26	0.23	0.00	3.84	1.72	0.06	−5.00	0.01
Third quartile	0.76	4.93	3.84	0.40	0.00	5.59	2.71	0.50	3.81	0.02
Variance	0.01	13.43	33.74	0.01	0.00	1.73	0.31	0.10	49.03	0.00
Average deviation	0.08	2.50	2.72	0.10	0.00	1.09	0.50	0.27	5.86	0.01
Standard deviation	0.11	3.71	5.88	0.12	0.00	1.33	0.57	0.32	7.09	0.01
Coefficient of variation	0.01	13.43	33.74	0.01	0.00	1.73	0.31	0.10	49.03	0.00
Skew	−1.63	2.73	4.43	0.24	0.58	−0.71	0.18	0.71	0.07	1.47
Kurtosis	3.56	9.78	21.06	−1.04	−1.71	0.01	−1.30	−0.65	−0.94	1.59

$$DDR = \left(\frac{\text{Predicted Value}}{\text{Observed Value}}\right) - 1 \tag{11}$$

In Equations (9) and (10), O, P = observational and predicted or output values, respectively. $\bar{O}$, $\bar{P}$ = Average observational and predicted data, respectively, and n = the number of samples.

Results of the MARS model

The preparation and development of the MARS model as stated in the material and methods section consists of two stages, the first stage includes the growth and development of the model and the second stage includes pruning the model. In the first stage, to explore the model space and fit the regression equations, they are divided into several subspaces, and in the second stage, some of them are pruned to prevent overfitting. To develop the MARS model to estimate the discharge in non-prismatic

compound channel, in the first stage, about 30 basis functions were prepared, and in the second stage (pruning stage) 10 of them were removed. The mathematical model obtained from the MARS model is presented in Equation (12). The functions and coefficients of this model are presented in Table 5. Evaluation of the MARS structure shows that: δ^*, S_o, β, A_r, and f_r had the greatest effects in the final mathematical model to estimate the discharge in CCNPF. The error statistics of the MARS model developed in the training and testing steps are shown in Figure 7. As shown in this figure, the statistical indices of this model in the training step are $R^2 = 0.986$ and RMSE = 0.002, and in the testing step are $R^2 = 0.962$ and RMSE = 0.003. In this model, the DDR index was also calculated and the corresponding diagram was prepared, which is shown in Figures 8 and 9. It can be seen from these figures, the range of DDR index changes in the training and testing step is between [−0.4, 0.3].

To determine whether this model has over-fitting or under-fitting properties, the DDR index histogram is plotted (Figures 8 and 9).

Assessment of these figures at the training and testing steps show that: the DDR histogram is not particularly skewed, and the MARS model has no significant overestimation or underestimation.

The survey of statistical indicators shows that the MARS model has a good performance for estimating the discharge in CCNPF. The results of the correlational analysis can be seen in Equation (12).

$$Q = 0.042 + \sum_{M=1}^{20} \beta_m F_i(x) \tag{12}$$

GMDH model results

To develop the GMDH model for estimating the discharge in CCNPF, the same data used in the training and testing steps of the MARS model were used. In the GMDH model, only two parameters are assigned to each neuron. There are 36 neurons in

Table 5 | The basic function of the developed mathematical model by MARS algorithm

BF functions	Coefficients
$BF1 = \max(0, \delta^* - 1.87)$	−0.035
$BF2 = \max(0, 1.87 - \delta^*)$	0.046
$BF3 = BF1 * \max(0, 0.0011 - S_o)$	33.067
$BF4 = \max(0, S_o - 0.00099)$	16.524
$BF5 = \max(0, 0.00099 - S_o)$	−533.352
$BF6 = BF1 * \max(0, \beta - 0.364)$	−0.062
$BF7 = BF1 * \max(0, 0.364 - Dr)$	0.034
$BF8 = \max(0, \theta + 1.91)$	−0.013
$BF9 = \max(0, -1.91 - \theta)$	0.006
$BF10 = BF1 * \max(0, -3.81 - \theta)$	−0.003
$BF11 = \max(0, \theta - 5.71)$	0.002
$BF12 = BF4 * \max(0, 0.708 - f_r)$	44.688
$BF13 = \max(0, \theta + 9) * \max(0, \delta^* - 4.17)$	−0.002
$BF14 = BF9 * \max(0, \delta^* - 3.96)$	0.004
$BF15 = BF9 * \max(0, 3.96 - \delta^*)$	−0.004
$BF16 = \max(0, \theta + 3.81)$	0.011
$BF17 = \max(0, 5.71 - \theta) * \max(0, 0.269 - Dr)$	−0.003
$BF18 = \max(0, \theta + 9) * \max(0, \delta^* - 3.91)$	0.003
$BF19 = BF16 * \max(0, 1.28 - A_r)$	0.007
$BF20 = BF16 * \max(0, f_r - 0.82)$	−0.236

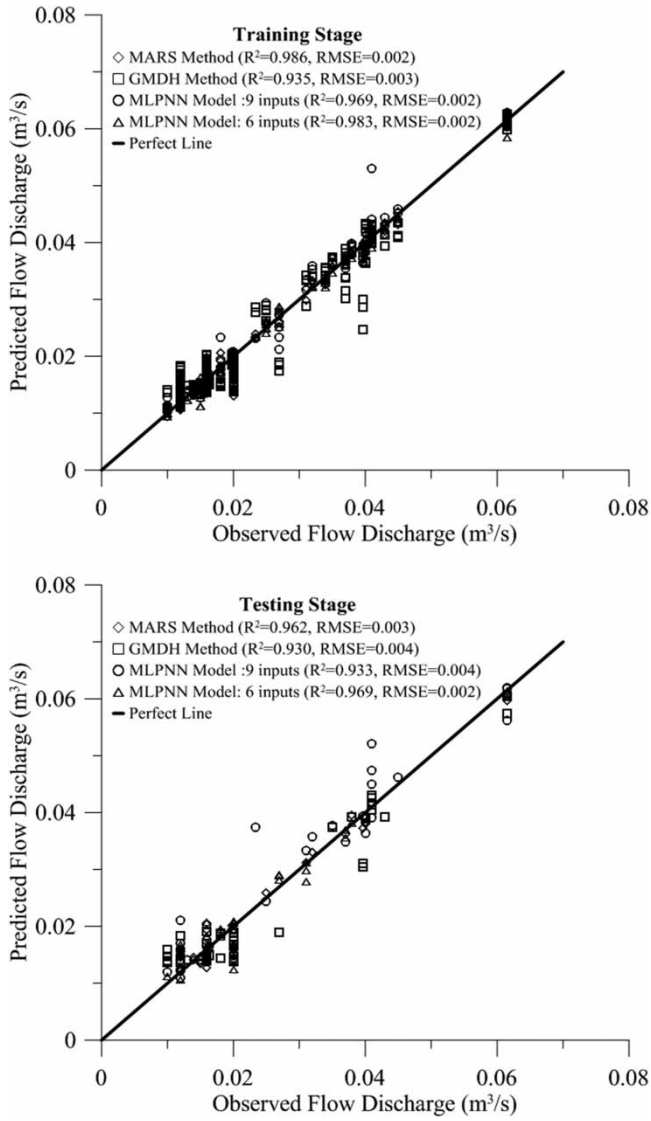

Figure 7 | The results of soft computing models in estimation of discharge in compound channel with non-prismatic flood plains.

the first layer of the GMDH model (Figure 3). Only neurons that have higher accuracy in estimating the discharge are selected and used in the construction of the next layer.

The coefficients of the activated function of the developed GMDH model are presented in Table 6. Evaluating the structure of the developed GMDH model shows that similar to the MARS model, this model has identified the parameters δ^*, S_o, Dr, and f_r as the most important parameters in estimating the discharge in CCNPF.

But instead of the A_r, the model has chosen the R_r, although there is a direct relationship between the A_r and R_r. The performance of the developed GMDH model in the training and testing steps is shown in Figure 7. As shown in this figure, the statistical indicators of GMDH model in the training step are $R^2 = 0.935$ and RMSE = 0.003 and in the testing step are $R^2 = 0.930$ and RMSE = 0.004, respectively. Comparison of the statistical indicators of the GMDH model with the MARS model shows that the GMDH model is partially less accurate. Also, the DDR index was calculated for this model. Its distribution diagram is plotted on the data used as well as its histogram (Figures 8 and 9). The range of DDR index changes for the GMDH model results in both training and testing steps varies between [−0.4, 0.5].

The scatter range of this model is larger than the MARS model. Examination of the DDR histogram of this model in the training step shows that this model has significantly overestimation. But in the testing step, the MARS model reduces this feature by dividing the space between input variables and regression modeling and provides more acceptable results.

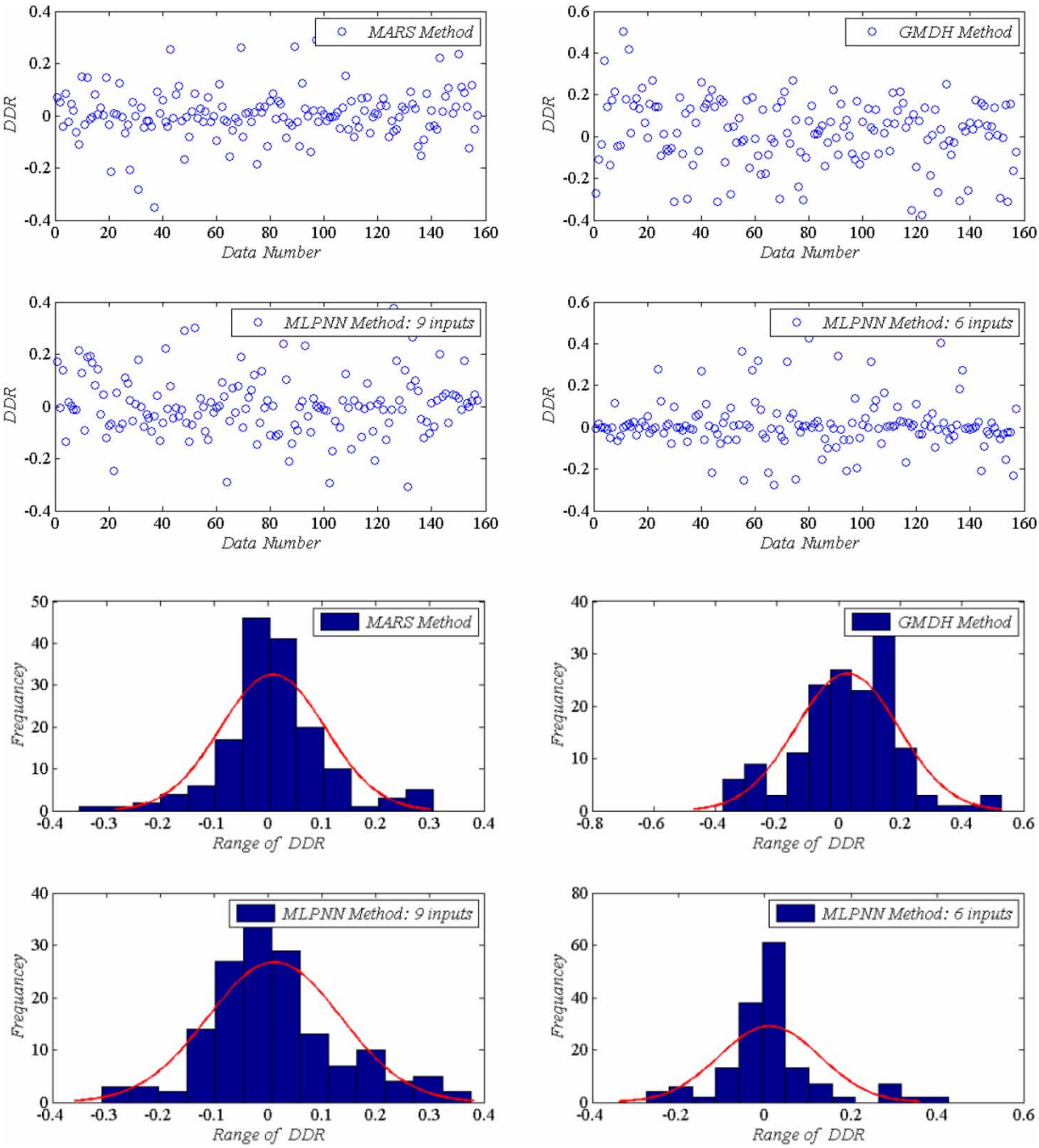

Figure 8 | DDR index for models in the training step.

Development of the MLPNN model

For the preparation of the MLPNN model, two strategies were used: considering all input parameters as the first model and then considering the most important parameters specified from the previous models as the input of the second model of input variables. The second strategy involves preparing two hidden layers for the network, each with five neurons. This strategy aimed to evaluate and compare the accuracy of the MLPNN model with the GMDH model. To use this model, a script has been written in Matlab software. To select the activation function, the types of functions embedded in this software

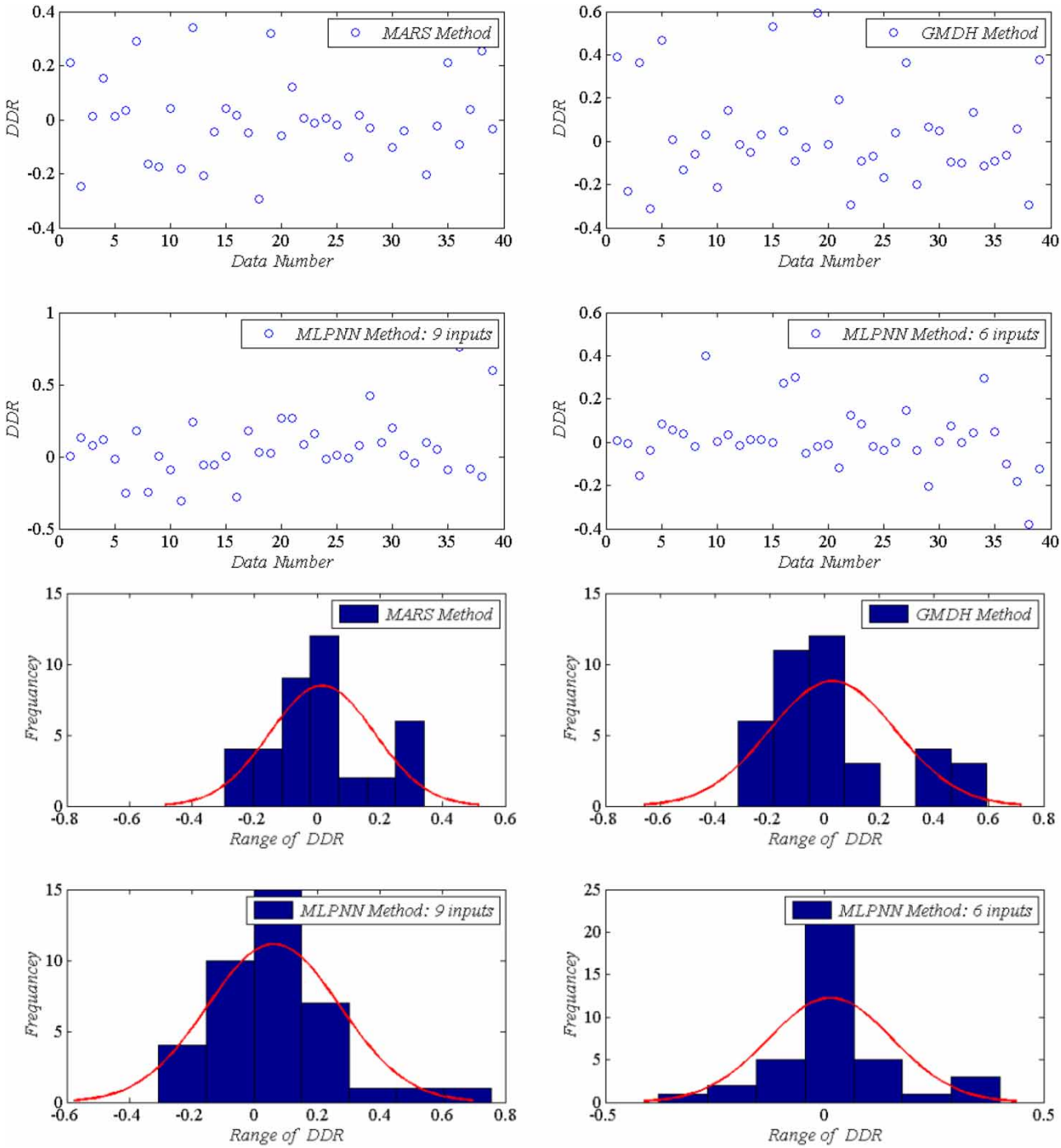

Figure 9 | DDR index of the models in the testing stage.

were examined and the result showed that the sigmoid tangent function has the best performance. The structure of the developed MLPNN model based on both scenarios is shown in Figure 10. Notably, the same data used for developing the MARS and GMDH models were used to develop the MLPNN model.

The performance of the MLPNN model developed at different stages of training and testing is shown in Figure 7. Examination of this figure shows that the statistical indices of error of the MLPNN model based on considering all the involved variables (9 variables) as input in the training stage are $R^2 = 0.969$ and RMSE = 0.002, and in the testing stage are $R^2 = 0.933$ and RMSE = 0.004. Also, the performance of the MLPNN model is calculated based on the most important parameters

Table 6 | The developed GMDH network coefficients to estimate discharge in non-prismatic compound channels

	b0	b1	b2	b3	b4	b5	b6
layer-1	−0.203	509.015	−0.047	−157,389.086	0.005	−6.383	0.004
	0.002	0.288	0.009	−0.267	−0.001	−0.039	0.005
	−0.027	0.299	−0.002	−0.209	0.000	−0.018	0.007
	0.093	−0.004	−0.022	0.000	0.001	0.002	0.007
layer-2	0.099	−0.027	−0.001	0.002	0.000	0.000	0.007
	0.004	0.528	0.155	−17.867	−30.246	53.195	0.004
	0.004	0.461	0.233	−15.991	−30.793	51.799	0.004
	−0.001	0.391	0.598	42.442	44.894	−86.729	0.004
	0.004	0.380	0.305	−5.786	−20.122	31.047	0.004
	−0.002	0.973	0.248	−40.516	−43.986	81.660	0.005

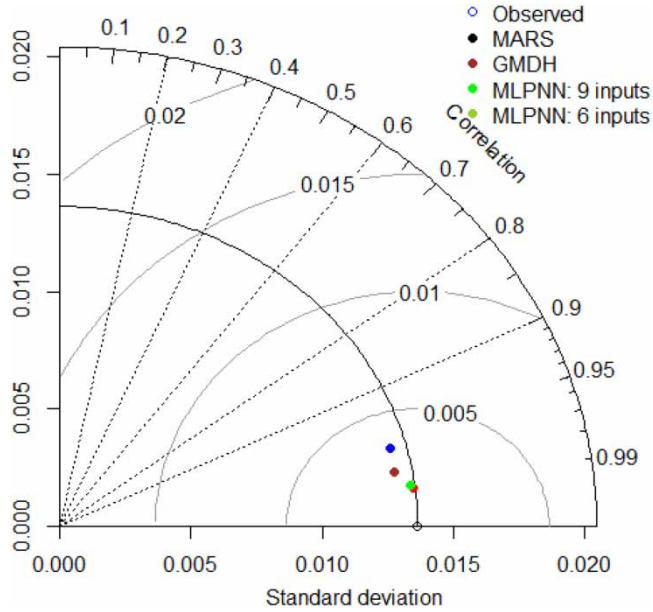

Figure 10 | Taylor diagram for comparison of performance in models used in the training stage.

as input (6 variables) and is shown in Figure 7. Examination of this figure shows that the error indices of the MLPNN model based on the most important influential variables in the training and testing step are $R^2 = 0.983$ and RMSE = 0.002 and $R^2 = 0.969$ and RMSE = 0.002. Examining the performance of the MLPNN model based on both scenarios shows that any additional information as model input not only does not increase the accuracy of the neural network model but also slightly decreases its accuracy. The Taylor diagram was used to comprehensively examine the developed models including MARS, GMDH, and MLPNN (based on both scenarios). The Taylor diagram for the training and testing stages is shown in Figures 10 and 11. As it shows, in the training stage, the performance of all models is almost equal to each other, but in the testing stage based on the taylor diagram that used the R^2 and RMSE indices, the performance of the GMDH model is significantly weaker.

Estimating discharge in main channel and floodplains

As mentioned, in flood engineering studies, it is important to estimate the discharge in the main channel and the floodplains. In this section, the contribution of each of the different parts of the compound channel including the main channel and non-prismatic floodplains of the total flow discharge is presented using the mentioned soft calculation models. Relative roughness parameters (f_r), convergence or divergence angle, relative depth, and relative distance were used as inputs of the mentioned models. The structure of the MARS model developed to estimate the share of the main channel of the flow discharge (Q_m) is

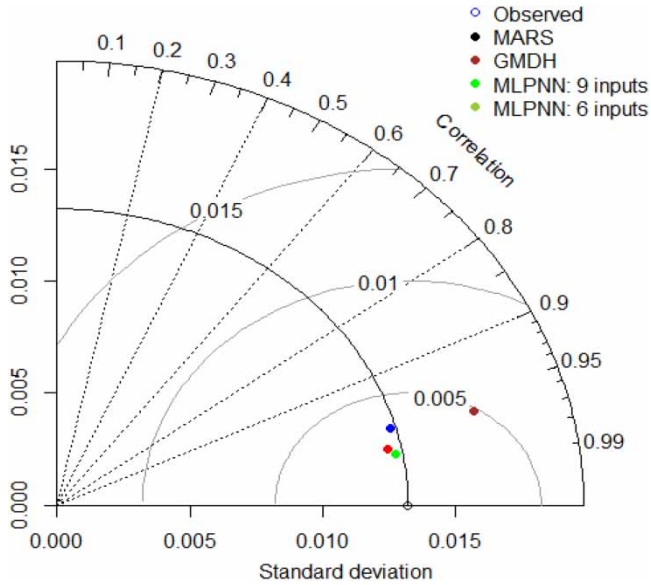

Figure 11 | Taylor diagram for comparison of performance in models used in the testing stage.

presented in Equation (13) and the extended form of the basis functions and their coefficients are presented in Table 7.

$$Q_m = 89.927 + \sum_{M=1}^{18} \beta_m F_i(x) \tag{13}$$

Table 7 | Basis functions and model coefficients developed for estimating Q_m

Basic functions	Coefficients
$BF1 = \max(0, x_r - 0.25) * \max(0, Dr - 0.35)$	−356.244
$BF2 = \max(0, x_r - 0.25) * \max(0, 0.35 - Dr)$	1,695.451
$BF3 = \max(0, \theta - 3.81)$	−1.257
$BF4 = \max(0, 3.81 - \theta)$	−1.803
$BF5 = \max(0, 0.35 - Dr)$	36.839
$BF6 = \max(0, x_r - 0.25) * \max(0, \theta + 3.81)$	−3.968
$BF7 = \max(0, x_r - 0.25) * \max(0, -3.81 - \theta)$	−0.902
$BF8 = \max(0, -3.81 - \theta)$	3.520
$BF9 = \max(0, \theta + 3.81) * \max(0, 0.5 - x_r)$	2.544
$BF10 = \max(0, x_r - 0.25) * \max(0, 0.4 - Dr)$	−741.817
$BF11 = \max(0, x_r - 0.25) * \max(0, 2 - f_r)$	−5.626
$BF12 = BF5 * \max(0, 0.5 - x_r)$	−67.410
$BF13 = \max(0, x_r - 0.25) * \max(0, 0.3 - Dr)$	−861.265
$BF14 = \max(0, x_r - 0.25) * \max(0, Dr - 0.25)$	429.220
$BF15 = BF4 * \max(0, Dr - 0.3)$	−9.656
$BF16 = BF4 * \max(0, 0.3 - Dr)$	11.211
$BF17 = BF5 * \max(0, -3.81 - \theta)$	−15.543
$BF18 = BF3 * \max(0, x_r + 0)$	4.091

The performance of the MARS model developed at different phases, including training and testing, is shown in Figure 12, respectively. The statistical indices of the developed model in the training stage are $R^2 = 0.986$ and RMSE = 1.320 and in the testing stage are $R^2 = 0.979$ and RMSE = 1.723.

In the following, the performance of GMDH and MLPNN models is presented and evaluated to estimate the contribution of the main channel cross-section in the convey of total flood discharge. The structures of the developed GMDH and MLPNN models are shown in Figures 13 and 14. The table of coefficients of the neurons involved in the GMDH network is also presented in Table 8. As can be seen from these figures, the statistical indices of GMDH and MLPNN models in the training stage are: $GMDH_{Training}$: $R^2 = 0.830$, RMSE = 4.592 and $MLPNN_{Training}$: $R^2 = 0.982$, RMSE = 1.595, respectively. In the testing stage are: $GMDH_{Test}$: $R^2 = 0.69$, RMSE = 5.412 and $MLPNN_{Test}$: $R^2 = 0.933$, RMSE = 2.183, respectively. A summary of the statistical indices of the models used is presented in Table 9. Evaluation of this table shows that the accuracy of the MARS model is higher than other models.

The performance of MARS, GMDH, and MLPNN models in the estimation of the contribution of floodplains from the total discharge passing (Q_f) is investigated. The basis functions and related coefficients are presented in Table 10. The performance

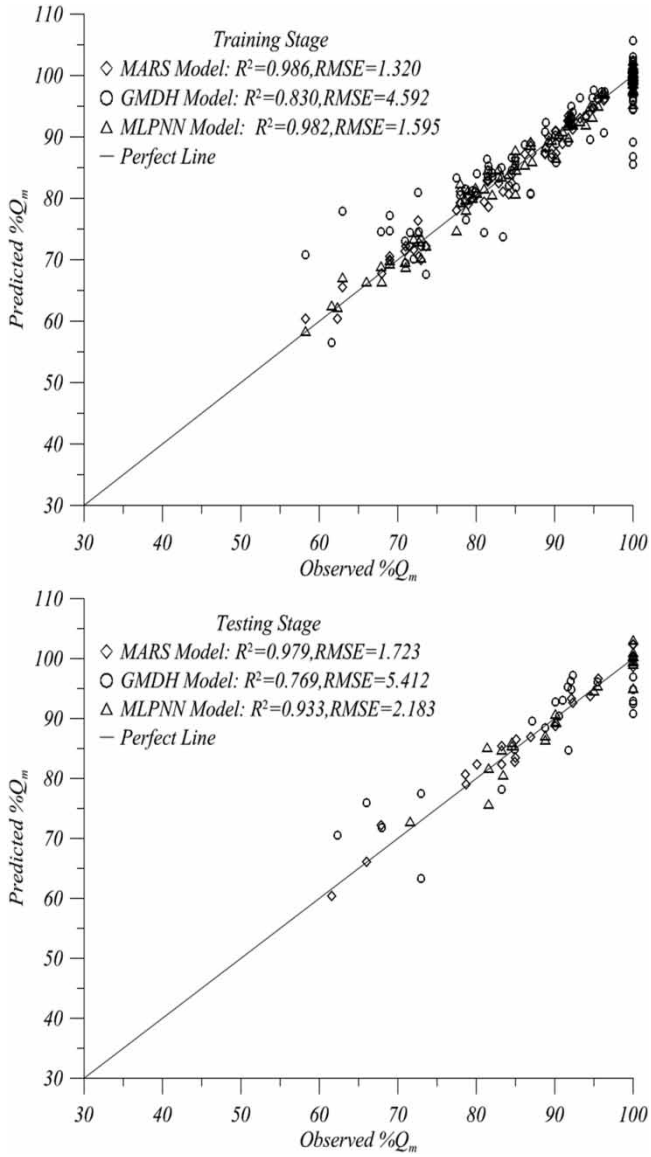

Figure 12 | Performance of models developed to estimate discharge in the main channel.

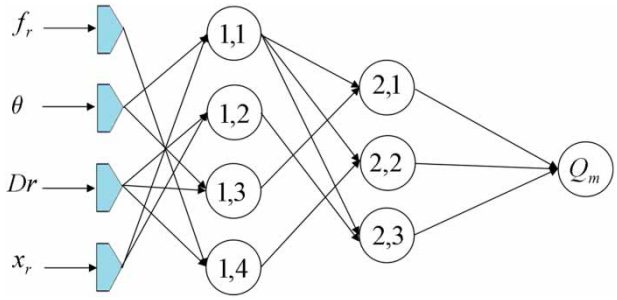

Figure 13 | The structure developed the GMDH model to estimate flow rate in the main section.

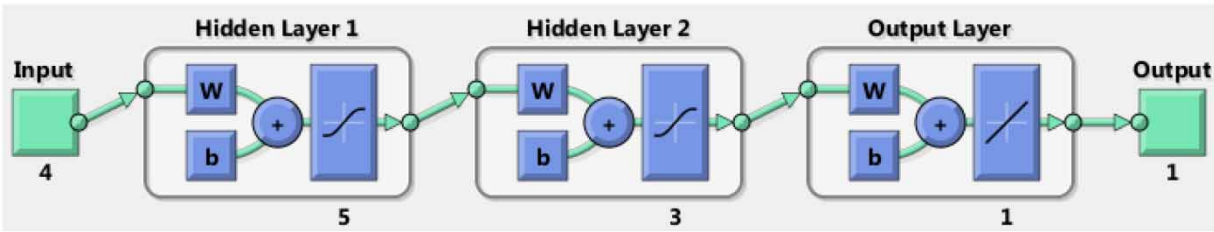

Figure 14 | The GMDH model structure developed to estimate discharge in main channel and floodplains.

Table 8 | The coefficients of developed GMDH network to estimate discharge in the main channel of the CCNPF

	b0	b1	b2	b3	b4	b5	b6
layer-1	90.751	1.253	−14.305	−0.014	14.378	−2.292	90.751
	116.271	−91.802	−39.201	33.262	15.473	63.203	116.271
	101.198	0.168	−44.835	0.009	4.407	−0.881	101.198
	108.542	−7.859	−66.635	2.689	55.058	−2.445	108.542
layer-2	−1,186.203	10.568	15.696	0.005	−0.023	−0.117	−1,186.203
	−985.800	6.668	15.201	0.014	−0.032	−0.092	−985.800
	−981.862	6.499	15.478	−0.005	−0.054	−0.053	−981.862
layer-3	−90.627	7.223	−4.243	0.180	0.240	−0.431	−90.627

Table 9 | Statistical indices of the models developed to estimate the discharge in the main channel

	Training Stage		Testing Stage	
Methods	**R^2**	**RMSE**	**R^2**	**RMSE**
MARS	0.986	1.320	0.979	1.723
GMDH	0.830	4.592	0.769	5.412
MLP	0.982	1.595	0.933	2.183

of the models in the training and testing stages is also shown in Figure 15.

$$Q = 18.823 + \sum_{M=1}^{22} \beta_m F_i(x) \tag{14}$$

Table 10 | Basis functions and coefficients of the MARS model developed for estimation of Q_f

Basis functions	Coefficients
$BF1 = \max(0, 0.4 - Dr)$	−130.933
$BF2 = \max(0, x_r - 0.25) * \max(0, \theta - 5.7)$	6.336
$BF3 = \max(0, 5.7 - \theta)$	−2.725
$BF4 = \max(0, Dr - 0.35)$	142.337
$BF5 = BF1 * \max(0, 0.25 - x_r)$	−317.615
$BF6 = \max(0, 2 - f_r)$	2.555
$BF7 = \max(0, 0.25 - x_r) * \max(0, \theta + 3.81)$	−5.756
$BF8 = \max(0, 0.25 - x_r) * \max(0, \theta - 3.81)$	6.965
$BF9 = \max(0, 0.25 - x_r) * \max(0, 3.81 - \theta)$	−6.096
$BF10 = \max(0, x_r - 0.25) * \max(0, \theta - 3.81)$	−6.254
$BF11 = \max(0, x_r - 0.25) * \max(0, -3.81 - \theta)$	5.274
$BF12 = \max(0, x_r - 0.25) * \max(0, Dr - 0.2)$	1,218.284
$BF13 = \max(0, x_r - 0.25) * \max(0, 0.2 - Dr)$	−2,068.526
$BF14 = \max(0, x_r - 0.25) * \max(0, Dr - 0.25)$	−1,470.058
$BF15 = \max(0, x_r - 0.25) * \max(0, 0.25 - Dr)$	1,880.897
$BF16 = BF3 * \max(0, 0.3 - Dr)$	−17.987
$BF17 = \max(0, 0.35 - Dr) * \max(0, x_r - 0.5)$	−318.956
$BF18 = \max(0, 0.35 - Dr) * \max(0, 0.5 - x_r)$	427.501
$BF19 = \max(0, 0.35 - Dr) * \max(0, 5.7 - \theta)$	12.529
$BF20 = BF3 * \max(0, x_r - 0.75)$	−7.267
$BF21 = BF3 * \max(0, 0.75 - x_r)$	5.216
$BF22 = \max(0, x_r - 0.25) * \max(0, f_r - 2)$	−5.471

The structure of the GMDH model developed to estimate the discharge passing in the floodplain is shown in Figure 16, and its associated coefficients are shown in Table 11. The structure of the neural network model is also shown in Figure 14. The error statistical indices of the developed models are generally presented in Table 12. This table shows that the MARS algorithm has the best accuracy.

Comparison with previous findings

The performance of computational models developed in this study was compared with the ANFIS developed by Dos *et al.* [22]. Also, comparison and investigation of these findings showed that the structure of MARS and GMDH models is consistent with the results of the gamma test. In other words, both the structure of the GMDH and MARS models and the gamma test confirm that the most important parameters involved in estimating the discharge in CCNPF are δ^*, S_o, Dr, A_r, f_r, and R_r. Examination of the error indices of the model developed with these two models shows that the ANFIS models in the test stage are: $R^2 = 0.850$, RMSE = 0.005. The comparison of the indices of the models developed in this research with ANFIS shows that the MARS and MLPNN models developed in this research can model and predict the discharge in CCNPF much more efficiently and accurately.

CONCLUSION

In the present study, the flow discharge (Q) in a CCNPF (convergent and divergent floodplains) was modeled and estimated using soft computational models including MARS, GMDH, and MLPNN models. For this purpose, the geometric and hydraulic characteristics of the flow include relative roughness (f_r), relative area (A_r), relative hydraulic radius (R_r), flow aspect ratio (δ^*), relative width (α), relative depth of the flow (Dr), relative longitudinal distance (x_r), the angle of convergence or divergence (θ) of the floodplain relative to the main channel (positive for divergence angle and negative angle for

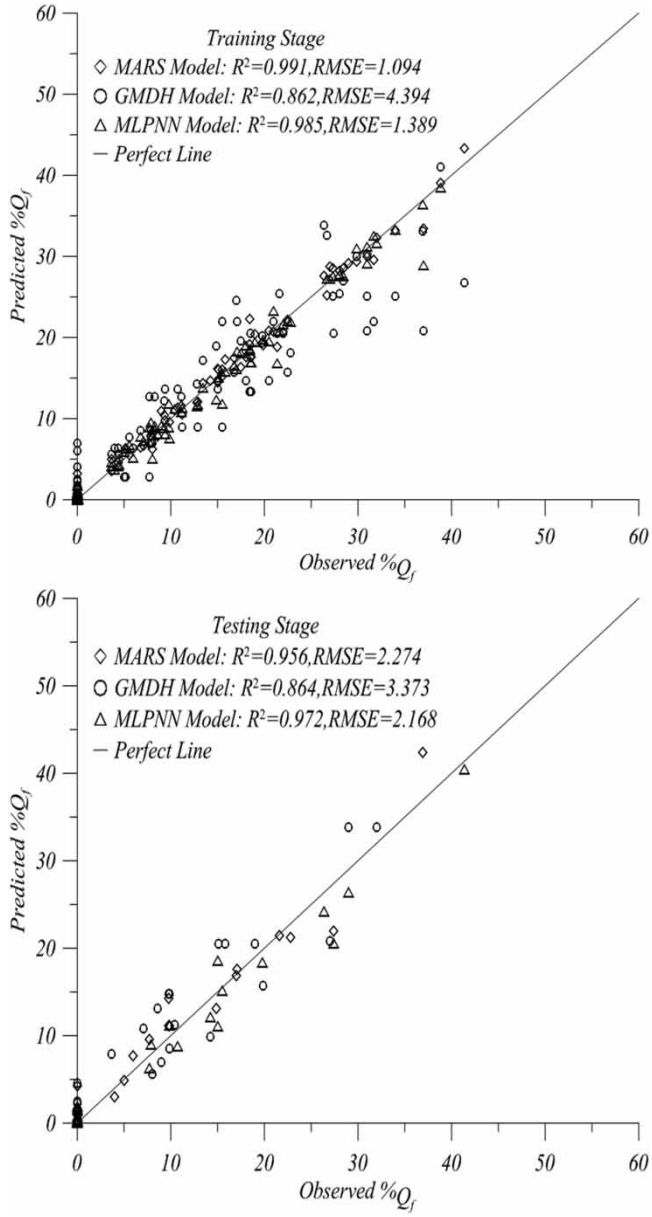

Figure 15 | Performance of models developed to estimate discharge passing in floodplains.

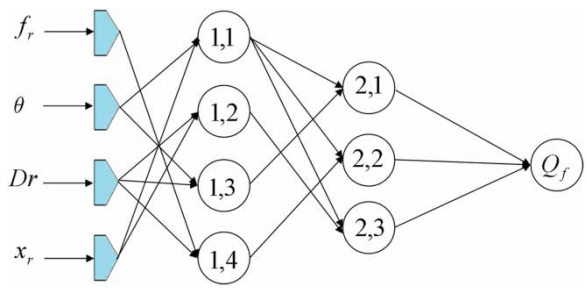

Figure 16 | GMDH model structure developed to estimate discharge passing in floodplains.

Table 11 | The coefficients of the developed GMDH model to estimate discharge passing in flood plains

	b0	b1	b2	b3	b4	b5	b6
layer-1	−25.836	132.501	40.987	−44.750	−11.453	−80.880	−25.836
	13.044	−1.595	12.901	−0.005	−15.060	2.482	13.044
	−2.322	1.445	53.251	−0.145	13.106	−5.925	−2.322
layer-2	−3.912	0.178	0.770	0.013	−0.009	0.021	−3.912
	−0.231	−0.763	1.666	0.036	−0.139	0.108	−0.231
layer-3	−2.085	1.026	0.223	0.002	0.003	−0.010	−2.085

Table 12 | Statistical indices of models developed to estimate discharge passing in floodplains

	Training Stage		Testing Stage	
Methods	**R^2**	**RMSE**	**R^2**	**RMSE**
MARS	0.991	1.094	0.956	2.274
GMDH	0.862	4.394	0.864	3.373
MLP	0.985	1.389	0.972	2.168

convergence) and S_0 as the bed slope were considered as inputs. Then, the performance of the developed models was compared with ANFIS (presented by previous researchers). The results of this study for global discharge in CCNPF showed that the statistical indices of MARS model error in the test stage are $R^2 = 0.962$, RMSE = 0.003 and the statistical indices of the GMDH model in this stage are $R^2 = 0.930$, RMSE = 0.004, and in the neural network model with a combination of the most important variables is $R^2 = 0.969$, RMSE = 0.002. It should be noted that the error indices of the ANFIS model in the test phase are $R^2 = 0.850$, RMSE = 0.005. Comparison of the performance of the mentioned models showed that the MARS model provides more accurate results than other models. Examination of the structure of GMDH and MARS models shows that the most important parameters influencing the discharge estimation are δ^*, S_o, Dr, A_r, f_r, and R_r. This result has been approved by previous researchers with the gamma test. In the following, the performance of utilized soft computing models used in modeling and estimating the share of each part of compound open channel including the floodplains and the main channel in the flood discharge was investigated. For this purpose, the parameters of D_r, x_r, convergence or divergence angle (θ), and relative roughness (f_r) were used as inputs. The results indicated that the MARS model with $R^2 = 0.979$, RMSE = 1.723 for predictive modeling of discharge in the main channel in the testing stage, and $R^2 = 0.956$, RMSE = 2.274 for discharge in floodplains has the best accuracy in comparison to other applied models.

DATA AVAILABILITY STATEMENT

If needed, the data can be made available to readers of the paper.

REFERENCES

Azamathulla, H. M. & Zahiri, A. 2012 Flow discharge prediction in compound channels using linear genetic programming. *Journal of Hydrology* **454**, 203–207.

Bhoria, S., Sihag, P., Singh, B., Ebtehaj, I. & Bonakdari, H. 2021 Evaluating Parshall flume aeration with experimental observations and advance soft computing techniques. *Neural Computing and Applications* **33**, 17257–17271.

Bousmar, D. 2002 Flow modelling in compound channels. Momentum transfer between main channel and prismatic or non-prismatic floodplains. *Unité de Génie Civil et Environnemental* **12**, 326.

Bousmar, D., Proust, S. & Zech, Y. 2006 Experiments on the flow in a enlarging compound channel Expériences d'écoulements dans un lit composé dont les plaines d'inondations s'élargissent. In: *3rd International Conference on Fluvial Hydraulics, River Flow 2006*, 6–8 September 2006, Lisbon, PRT, Oxford, UK. 576. 323–332.

Das, B. S., Devi, K., Khuntia, J. R. & Khatua, K. K. 2020 Discharge estimation in converging and diverging compound open channels by using adaptive neuro-fuzzy inference system. *Canadian Journal of Civil Engineering* **47** (12), 1327–1344.

Dingman, S. L. 2009 *Fluvial Hydraulics*. Oxford University Press, Oxford, UK.
Friedman, J. H. 1991 Multivariate adaptive regression splines. *The Annals of Statistics* **19** (1), 1–141.
Graf, W. H. & Altinakar, M. 1998 *Fluvial Hydraulics: Flow and Transport Processes in Channels of Simple Geometry*. Wiley, New York.
Ivakhnenko, A. G. 1971 Polynomial theory of complex systems. *IEEE Transactions on Systems, Man, and Cybernetics* **1** (4), 364–378.
Knight, D. & Demetriou, J. 1983 Flood plain and main channel flow interaction. *Journal of Hydraulic Engineering* **109** (8), 1073–1092.
Mohanta, A. & Patra, K. C. 2021 Gene-expression programming for calculating discharge in meandering compound channels. *Sustainable Water Resources Management* **7** (33), 1–19.
Mohanta, A., Patra, K. & Pradhan, A. 2020 Enhanced channel division method for estimation of discharge in meandering compound channel. *Water Resources Management* **34** (3), 1047–1073.
Mohanty, P., Khatua, K. K. & Patra, K. C. 2011 *Investigation on Shear Layer in Compound Channels*. 16th National Conference Hydraulic and Water Resources (HYDRO) 2011.
Naik, B. & Khatua, K. K. 2016 Boundary shear stress distribution for a converging compound channel. *ISH Journal of Hydraulic Engineering* **22** (2), 212–219.
Naik, B., Khatua, K. K., Sahoo, R. & Satapathy, S. S. 2014 Flow analysis for a converging compound channel. *International Journal of Applied Engineering Research* **9** (2), 133–138.
Naik, B., Khatua, K. K., Wright, N., Sleigh, A. & Singh, P. 2017 Numerical modeling of converging compound channel flow. *ISH Journal of Hydraulic Engineering* **24** (3), 1–13.
Najafzadeh, M. & Azamathulla, H. M. 2015 Neuro-Fuzzy GMDH to predict the scour pile groups due to waves. *Journal of Computing in Civil Engineering* **29** (5), 04014068:1–8.
Najafzadeh, M. & Sattar, A. A. 2015 Neuro-Fuzzy GMDH approach to predict longitudinal dispersion in water networks. *Water Resources Management* **29** (7), 2205–2219.
Najafzadeh, M. & Zahiri, A. 2015 Neuro-Fuzzy GMDH-Based evolutionary algorithms to predict flow discharge in straight compound channels. *Journal of Hydrologic Engineering* **20** (12), 04015035:1–14.
Najafzadeh, M., Barani, G.-A. & Azamathulla, H. M. 2013 GMDH to predict scour depth around a pier in cohesive soils. *Applied Ocean Research* **40**, 35–41.
Othman, F. 2000 *Flow Modelling in Compound Channels*. University of Newcastle upon Tyne, Newcastle, UK.
Parsaie, A. & Haghiabi, A. H. 2017 Mathematical expression of discharge capacity of compound open channels using MARS technique. *Journal of Earth System Science* **126** (20), 1–15.
Parsaie, A., Najafian, S. & Yonesi, H. 2016 Flow discharge estimation in compound open channel using theoretical approaches. *Sustainable Water Resources Management* **2** (4), 359–367.
Parsaie, A., Yonesi, H. & Najafian, S. 2017 Prediction of flow discharge in compound open channels using adaptive neuro fuzzy inference system method. *Flow Measurement and Instrumentation* **54**, 288–297.
Pradhan, A. & Khatua, K. K. 2019a Discharge estimation at the apex of compound meandering channels. *Water Resources Management* **33** (10), 3469–3483.
Pradhan, A. & Khatua, K. K. 2019b Discharge prediction in meandering compound channels. *International Journal of Water* **13** (3), 209–220.
Rezaei, B. & Knight, D. W. 2009 Application of the Shiono and Knight Method in compound channels with non-prismatic floodplains. *Journal of Hydraulic Research* **47** (6), 716–726.
Roushangar, K., Nouri, A., Shahnazi, S. & Azamathulla, H. M. 2021 Towards design of compound channels with minimum overall cost through grey wolf optimization algorithm. *Journal of Hydroinformatics* **23** (5), 985–999.
Sellin, R. H. J. 1964 A laboratory investigation into the interaction between the flow in the channel of a river and that over its flood plain. *La Houille Blanche* **7**, 793–802.
Shiono, K. & Knight, D. W. 1989 Transverse and vertical Reynolds stress measurements in a shear layer region of a compound channel. In: *Proceedings of 7th Symposium Turb. Shear Flows*, Stanford, CA, USA, 1–6
Shiono, K. & Knight, D. W. 1991 Turbulent open-channel flows with variable depth across the channel. *Journal of Fluid Mech.* **222**, 617–646.
Sihag, P., Pandhiani, S. M., Sangwan, V., Kumar, M. & Angelaki, A. 2021 Estimation of ground-level O_3 using soft computing techniques: case study of Amritsar, Punjab State, India. *International Journal of Environmental Science and Technology*, 1–8.
Singh, P. & Tang, X. 2020 Estimation of apparent shear stress of asymmetric compound channels using neuro-fuzzy inference system. *Journal of Hydro-Environment Research* **29**, 96–108.
Singh, P., Tang, X. & Rahimi, H. R. 2019 Estimation of apparent shear stress of asymmetric compound channels using neuro-fuzzy inference system. *Journal of Hydrologic Engineering (ASCE)* **24** (12), 1–17.
Torfi, K., Albaji, M., Naseri, A. A. & Nasab, S. B. 2021 An introduction to the ancient irrigation structures upon Karun River in Shushtar City, Iran. *Iranian Journal of Science and Technology, Transactions of Civil Engineering* **45**, 815–831.
Yonesi, H. A., Omid, M. H. & Ayyoubzadeh, S. A. 2013 The hydraulics of flow in non-prismatic compound channels. *J Civil Eng Urban* **3** (6), 342–356.

First received 23 September 2021; accepted in revised form 4 February 2022. Available online 18 February 2022